G. Aridon
D. Rémond
F. Morestin
LaMCoS,
CNRS UMR 5259,
INSA-Lyon,
Lyon F-69621, France

L. Blanchard
Thales Alenia Space,
F-06156 Cannes La Bocca,
France

R. Dufour
LaMCoS,
CNRS UMR 5259,
INSA-Lyon,
Lyon F-69621, France
e-mail: regis.dufour@insa-lyon.fr

Self-Deployment of a Tape-Spring Hexapod: Experimental and Numerical Investigation

In the framework of developing a future space telescope, this paper focuses on a deployable hexapod equipped with tape-spring coiling devices. It describes the measurement of the platform deployment with a gravity compensation setup. The deployment modeling starts with the formulation of a phenomenological model for a single deployable coiling device. A force-elongation model is built experimentally by measuring the restoring force of such a hysteretic tape-spring actuator. Then, six actuator models are used in parallel to build a complete model of the deployable hexapod. Finally, measured and predicted platform responses are compared. A design of experiments approach highlights that disparities in the restoring force of tape-spring actuators are decisive for deployment success. A regression model is obtained to predict the hexapod's twist behavior, which is the main indicator of deployment failure. This investigation underlines the requirement of actuator control during deployment. [DOI: 10.1115/1.3042148]

1 Introduction

A number of significant technological developments for deployable structures are being studied and developed for future space programs. Deployable space structures offer several advantages such as lightweight and minimum stored volume during launch. However, once in space, they have to be deployed with the accuracy required by optical applications. Numerous concepts based on various technologies have been designed and have varying deployment accuracies and dynamic behaviors: inflatable structures [1], membrane structures [2], tape-spring hinges, and tensegrity structures [3]. After the deployment stage, these structures have to be corrected, for example, with mechanical actuators to permit image acquisition and the use of adaptive optics to reach the full performance of the instrument.

Parallel manipulators provide several advantages over serial architectures such as greater load carrying capability, high stiffness, and multiple positioning axes. An exhaustive overview of different types of parallel structures was presented by Merlet [4] for vehicle ride simulators, space- and ground-based telescopes, antennae, medical robots, etc. Moreover, in order to assume an optimal design, Merlet [5] clarified the significance of the Jacobian matrix, manipulability, and condition number. It is well known that stability requires a hexapod workspace free of singularity. Jiang and Gosselin [6] proposed a numerical algorithm to compute the maximal singularity-free workspace of the Gough–Stewart platform.

Thales Alenia Space designed a prototype of a deployable telescope in order to stow the secondary mirror during launch and to self-deploy it in orbit [7]. The structure is based on a hexapod whose legs are six deployable rolled tape-springs. When the stowing mechanism is released, the six legs autonomously bring the secondary mirror into its final position by reaching their full length configuration. After deployment, six vertical actuators located at the base correct deployment deviations along six degrees of freedom [8]. Second order deviations are corrected by using adaptive optics to reach the full performance of the instrument (see Fig. 1).

The hexapod self-deployment is achieved by the use of coilable tape-springs based on the tape-measure principle (see Fig. 2). A tape-spring is a thin curved metallic strip capable of keeping its straight configuration. Its bending moment has been fully investigated [9–11] to characterize their nonlinear behavior. In this application, the specific tape-spring coiling devices take on the role of prismatic actuators for deployment [12].

In a previous investigation [13], the deployment repeatability of a hexapod prototype was measured to within 10 μm accuracy by using photogrammetry on a series of 23 deployments: maximal translational and rotational deviations were 240 μm and 820 μrad in the final deployed position for a full deployment of 40 cm. Unlike these good performances, it appeared that the deployment process of the 652 mm height structure was not perfectly smooth during the tests. This is probably due to imperfections in the mounting part and positioning, which affect the dry friction of the linear actuators. This point leads to the conclusion that the deployment process has to be investigated with prediction tools in order to guarantee a secure deployment.

The first part of this paper is devoted to the description of the experimental setup dedicated to the measurement of the hexapod deployment with compensated gravity. To obtain a reliable dissipative model, the main stage consists in testing components and formulating a model based on this information. The experimental identification of the linear actuator is the main topic of the second part of the paper. Harmonic force-elongation loops are recorded for different elongation amplitudes and forcing frequencies. The hysteretic phenomena brought into play are highlighted. Thus, based on these measurements, a force-elongation model is identified to describe the behavior of the tape-spring linear actuators. Then, this single degree-of-freedom (DOF) actuator model is implemented in each leg of the hexapod to develop a complete nonlinear dynamic model of deployment. Finally, the response of the platform can be compared with both numerical and experimental approaches. Concluding remarks are provided with several recommendations on the parameter dispersion in the actuators by using the design of experiments (DOE) method.

Contributed by the Mechanisms and Robotics Committee of ASME for publication in the JOURNAL OF MECHANICAL DESIGN. Manuscript received December 10, 2007; final manuscript received October 7, 2008; published online January 6, 2009. Review conducted by Pierre M. Larochelle.

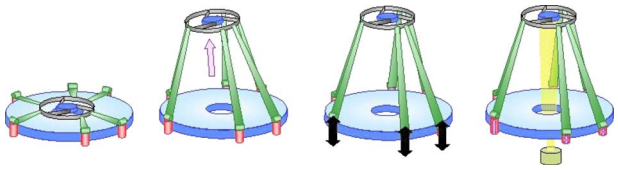

Fig. 1 Deployment concept: stowed configuration, deployment, correction stage, and adaptive optics

2 Deployment Tests

The aim is to carry out deployment tests with compensated gravity in order to investigate the behavior of the self-deployable prototype.

2.1 Gravity Compensation Setup. The developed setup, shown in Fig. 3, is able to provide several functions. The compensation of the gravity is achieved by using an equivalent mass with a pulley system. The manipulation of the prototype is delicate. Due to the sensitivity of the tape-spring hexapod, initial conditions have to be reproducible: the platform is maintained in its stowed configuration with a cable positioning it on a centering tube. The initial deployment height can change depending on the tube length. The platform is released by burning the cable with a match in order to ensure a minimum of dispersion in the initial conditions. In the case of accidental collapse of the platform, the tape-spring prototype would be irreversibly damaged. Thus, handrail rods provide a safe workspace of deployment paths. They are only there to prevent damage if the hexapod does not deploy properly. Normally it does not touch the handrails. Another function of the setup is to damp the end of the platform stroke. Indeed, the end-stop mechanisms of coiling devices have a high stiffness inducing a shock at the end-stroke, which could lead to tape-spring buckling. Since end-stroke optimization is not the aim of this study, the following will focus on the deployment phase.

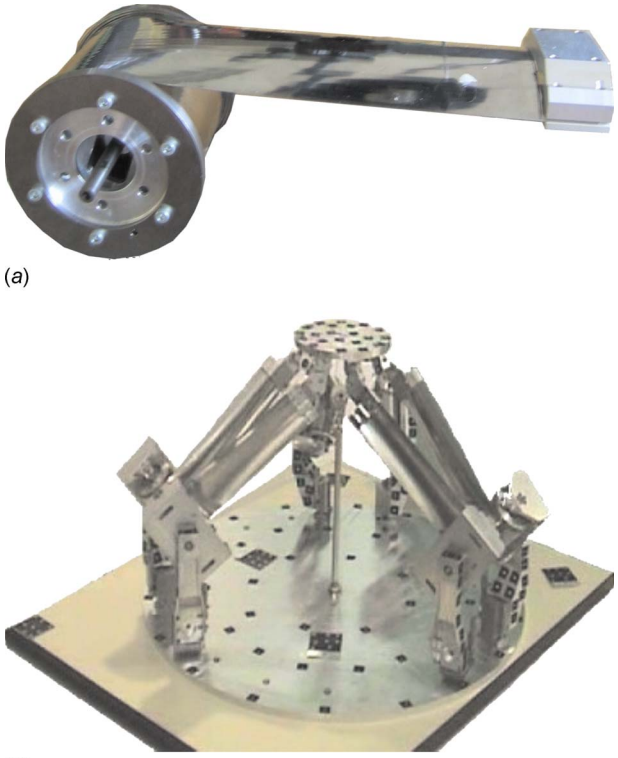

(*a*)

(*b*)

Fig. 2 Description of the hexapod design: (*a*) tape-spring coiling device; (*b*) tape-spring hexapod prototype

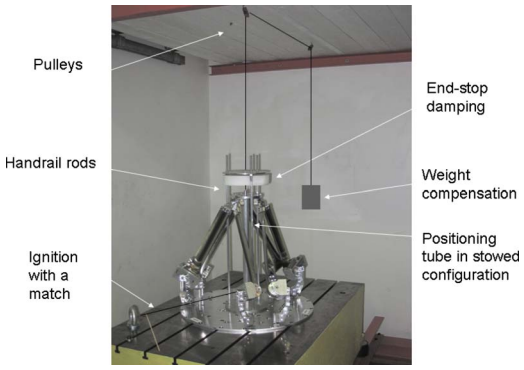

Fig. 3 Gravity compensation setup

Platform trajectory is recorded by high speed camera with a capacity of 1000 frames/s. Good resolution and a satisfactory field of view are achieved by reducing this to 250 frames/s (Fig. 4).

2.2 Exploitation With Digital Image Correlation Method. A digital image correlation method promises acceptable contactless displacement measurement. It could be used for all applications that require the acquisition of planar displacement and strain field information. The ICASOFT software [14] was used. It scans the final image toward the maximal correlation of the pixel pattern of reference. The platform perimeter is marked in order to facilitate image processing. Image gray levels are interpolated to improve measurement accuracy.

Figures 5 and 6 present measurements from two consecutive deployment tests. The quality of the recorded images did not permit test 2 to be resolved to maximum extension. A dispersion of about 5% between the two tests is noted. Lateral deviations are about 1.7 cm. It should be mentioned that no contact occurred between the handrail rods and the platform. Lateral deviations illustrate unequal tape-spring actuator lengths or bad initial conditions of the platform. This means that the hexapod is very sensitive despite precautions.

3 Modeling of the Tape-Spring Actuator

3.1 Experimental Identification. Linear actuators contain a rotating roll module with a spiral groove in order to guide the tape-spring. The coiling of the tape-spring causes its natural curved section to flatten (see Fig. 2(*a*)). Because of the stress generated by the elastic deformation, the tape-spring tends to self-unwind in order to recover its natural curved section.

This type of linear actuator is characterized by two main phenomena: the energy supplied by the deformation of the tape-spring (this concerns the transition zone between the flattened section and the naturally curved section of the tape-spring) and the energy dissipated due to the radial friction of the tape-spring at the entry of the spiral groove.

Instead of fastidiously modeling both phenomena, the strategy adopted consists in considering the actuator as a whole system and measuring the restoring force for different operating conditions. Figure 7(*a*) shows the experimental setup. The hub of the spool is fixed on a frame, making it possible to change the length of the unrolled tape-spring. The spool is free to rotate. The unrolled end of the tape-spring is connected to a load sensor and is sinusoidally excited by an electrodynamic shaker. The forced amplitude displacement, i.e., the elongation, is measured by using a laser sensor having a 10 μm accuracy.

Force-elongation loops are recorded for several forcing frequencies and unrolled strip lengths. They exhibit a nonlinear hysteretic behavior. The order of magnitude of the differential loads is about 0.1 N. The system supplies restoring force due to the stored strain energy of the rolled tape-spring. Figure 7(*b*) shows that the

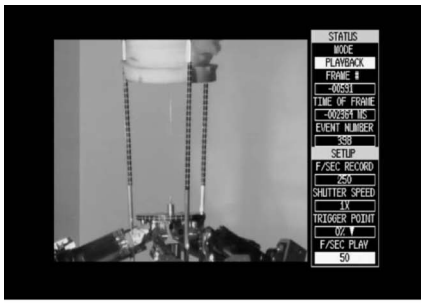

(*a*)

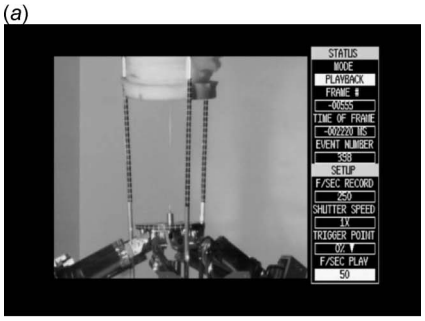

(*b*)

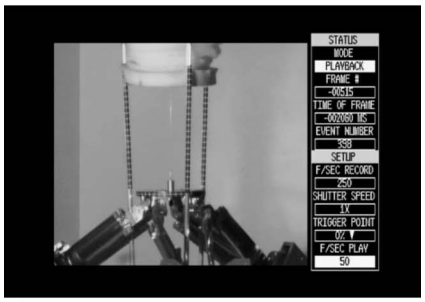

(*c*)

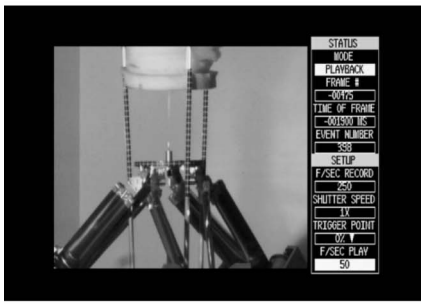

(*d*)

(*e*)

Fig. 4 Deployment sequence with compensated gravity: (*a*)–(*e*) represent positions at successive 144 ms intervals

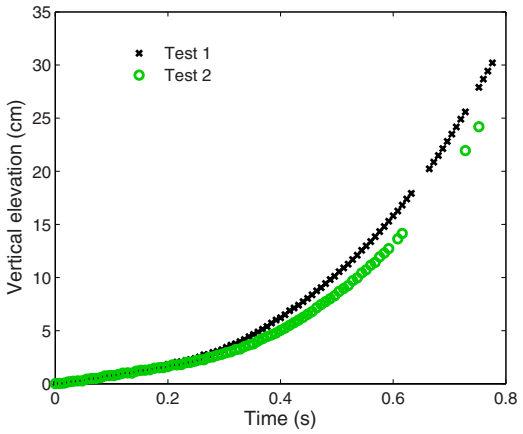

Fig. 5 Time history of measured platform elevations

path takes an anticlockwise direction: the self-unrolling load provided by the tape-spring is lower than the load required to roll it on the hub. Both measured loads are positive because the tape-spring is preloaded.

It appears that the unrolled and rolled forces remain quite constant whatever the range of elongation is (see Fig. 8(*a*)). This is due to the strain energy provided by the transition zone of the deformed tape-spring (Fig. 9), which remains constant at any length of deployment over 0.25 m. The rolled part of the tape-spring in the spiral groove has no influence on the restoring force and could be considered as clamped. This assumption based on an independent transition length for tape-spring overall length was verified experimentally (see Fig. 8(*b*)).

3.2 A Dynamic Restoring Force Model. Kinetic friction can be modeled by Coulomb's theory, but the transition from static to kinetic friction is unrealistic as discontinuity at zero displacement implies an infinite rate of change of force, which is not physically reasonable. Thus the model is satisfactory for high magnitudes of sliding friction, but it gives an incomplete description of the frictional behavior at low magnitude. In 1976 [15], Dahl proposed a dynamic model to avoid discontinuity. It is best described as a position dependent friction model rather than a velocity dependent model. On the basis of the Dahl model, Al Majid and Dufour proposed in Ref. [16] a more general restoring force model. Adapted to the device studied here, it is described by the following first order differential equation:

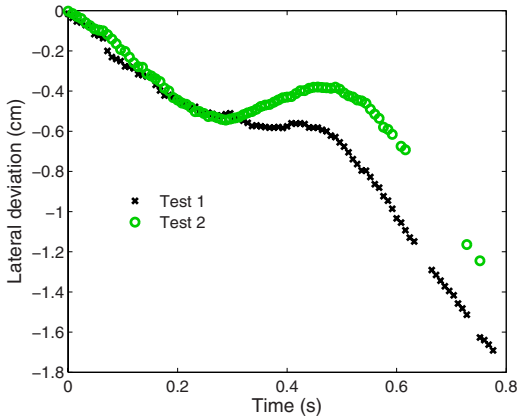

Fig. 6 Time history of measured lateral deviations of the platform

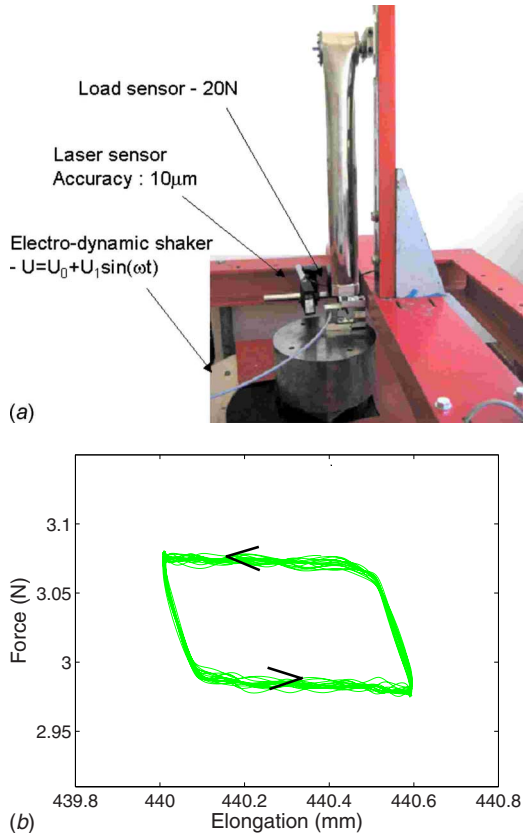

Fig. 7 (*a*) Experimental setup. (*b*) Hysteresis loops at 1 Hz.

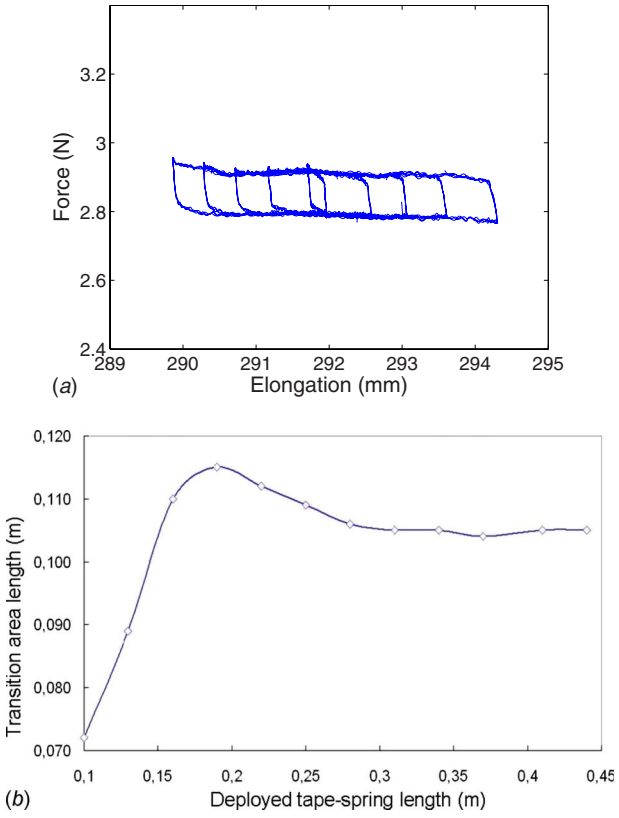

Fig. 8 (*a*) Loops for different elongations at 0.2 Hz. (*b*) Transition zone versus deployed tape-spring length.

$$\dot{R} = \beta \dot{u} |h - R\ \mathrm{sgn}(\dot{u})| \tag{1}$$

where R is the restoring force, u is the longitudinal elongation of the tape-spring, and β is a parameter that adjusts the shape of the friction slope function. The hysteretic behavior is captured by defining function h, so that

$$h = \frac{(h_u + h_l)\mathrm{sgn}(\dot{u}) - (h_u - h_l)}{2} \tag{2}$$

where h_u and h_l represent, respectively, the upper and lower asymptotic curves of the loop and make the Dahl model as general as possible [17,18].

The tests, presented in Sec. 2, permit updating the parameters of such a phenomenological model. The equations of both the upper and lower asymptotic boundaries are identified, thanks to the least-squares method. It appears that h_u and h_l can be approximated by straight lines (dashed lines in Fig. 10),

$$h_l = a_l u + b_l \tag{3}$$

$$h_u = a_u u + b_u \tag{4}$$

Constants a_l, b_l, a_u, and b_u are the slopes and the initial forces of uncoiling and coiling, respectively. Parameter β is identified by comparing the theoretical and experimental dissipated energies, i.e., the loop areas [19]. Figure 10 compares steady state measured and simulated force-elongation loops. The simulated loop is obtained by using a step-by-step time integration method with an initial deployment force of 2.987 N corresponding to the effort stored by the actuator in the prestress part of the tape-spring.

3.3 Dynamic Effects. Force-elongation loops were also recorded for several forcing frequencies. It should be noted that the level of the efforts is very low, leading to measurement difficulties and to dynamic effect sensitivity. Consequently, dynamic effects have to be considered even for an excitation at 3 Hz. Figure 11 depicts the responses of the actuator at two forcing frequencies (1 Hz and 3 Hz) and shows that dynamic effects, mostly due to the hub inertia, cause the hysteretic loop rotation.

Thus the hub inertia is taken into account in Al Majid's model, thanks to the possibility given by the asymptotic curves, which depend on the forcing frequency. Based on experimental data, Fig. 12 shows the evolution of the straight line equation parameters versus cycling velocity.

Second order polynomial equations approximate the two curves. They were implemented in the h function of the restoring force model in order to take into account the hub dynamics.

In order to identify the origin of the dynamic effects, the influence of hub inertia was subtracted from the measured forces. The aim was to distinguish the dry friction of the tape-spring in the groove from viscous friction provided by the internal roller bear-

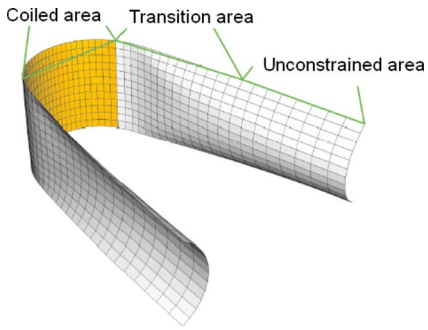

Fig. 9 Transition area of a flattened tape-spring

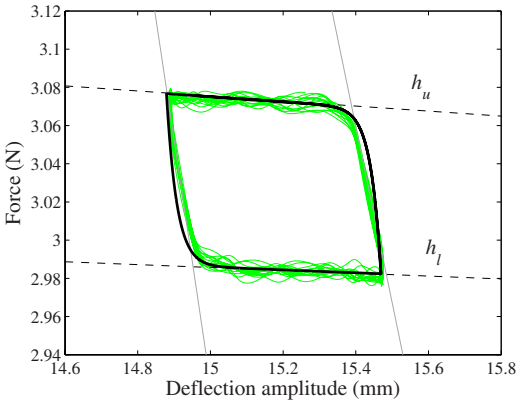

Fig. 10 Measured and simulated force-elongation loop of the actuator

ing supporting the hub axis. Using a typical formula peculiar to such hysteretic behavior, such as effective stiffness K_{eff}, can provide reliable trends,

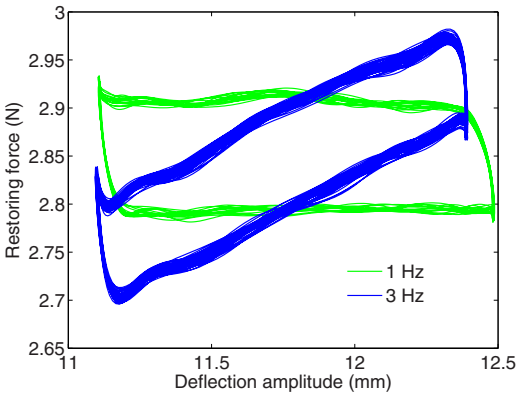

Fig. 11 Influence of hub inertia

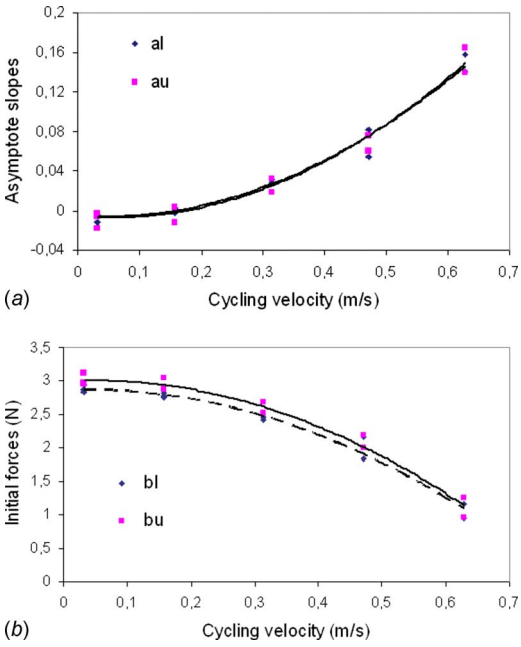

Fig. 12 Evolution of the coefficients of the straight asymptotic lines. (*a*) Initial force. (*b*) Asymptote slope.

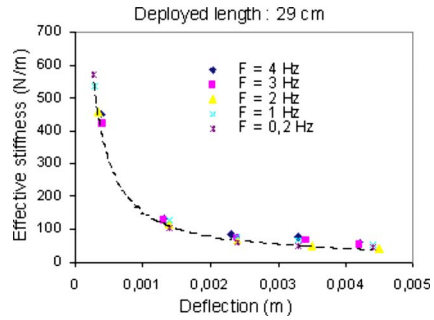

Fig. 13 Effective stiffness versus longitudinal elongation for different forcing frequencies

$$K_{\text{eff}} = \frac{F_{\max} - F_{\min}}{X_{\max} - X_{\min}} \tag{5}$$

Plotting measured effective stiffnesses versus elongation amplitudes [20] for different sets of forcing frequencies (shown in Fig. 13) indicates that frequency dependence is negligible. It proves that the major dissipative effect is dry friction caused by flange spiral groove-strip contact. Thus the tape-spring actuator is equivalent to a stick-slip system.

4 Modeling the Deployable Hexapod

The tape-spring hexapod was designed as a Gough–Stewart parallel robot: each leg is equipped with a passive spherical joint and a universal joint linked to the platform and the base-plate, respectively. The hexapod model is composed of an upper platform linked to the base by six actuators with prismatic joints (see Fig. 14). The motion of the prismatic joints is controlled by the Al Majid model presented previously. The evolution of the boundary asymptotes with the cycling velocity presented in Sec. 3.3 is implemented in the h function of the restoring force model.

The model of the hexapod is implemented on SIMMECHANICS, a MATLAB toolbox that performs the forward dynamic analysis of the manipulator using the recursive Newton–Euler technique (see Fig. 15). Usually, the forward dynamic analysis cannot be easily solved analytically on a hexapod because of the closed-kinematic chain and the leg couplings. Both numerical and analytical approaches have been compared in Ref. [21].

Values of Cartesian and angular deviations Δ_x, Δ_y, Δ_z, $\Delta\theta_x$, $\Delta\theta_y$, and $\Delta\theta_z$ are collected as output values and plotted as functions of time. End-stops are modeled by adding springs and dampers leveled with an error function.

4.1 Experimental and Numerical Investigation. The experimental system of gravity compensation as it is designed does not

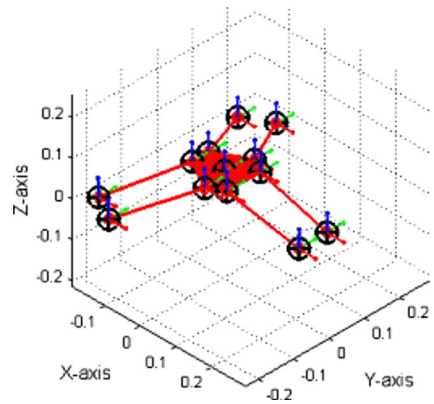

Fig. 14 Sketch of the parallel hexapod

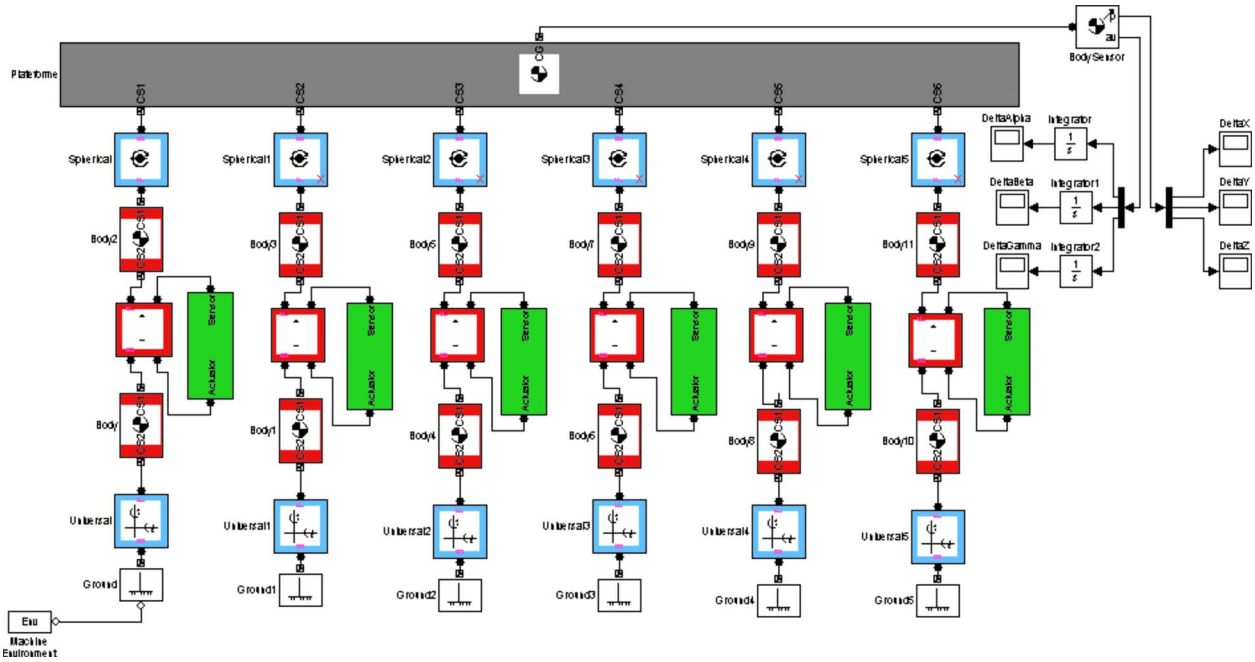

Fig. 15 Architecture of the hexapod model with SIMMECHANICS

reproduce zero-gravity conditions. Indeed, the equivalent mass compensates the platform weight by nullifying potential energy but doubles the kinetic energy of the system. Thus, in the following parts of the paper, the effective platform mass (m) is doubled in the models in order to reproduce the same environment conditions as those of the setup. The prediction of the gravity influence on the deployment is illustrated in Fig. 16 on which are plotted platform elevations with gravity ($g=9.81$ m/s^2 and $m=0.8$ kg), with compensated gravity ($g=0$ m/s^2 and $m=1.6$ kg), and without gravity ($g=0$ m/s^2 and $m=0$ kg). For the demonstration, these simulations are carried out with actuator restoring forces four times greater than those used in the prototype. If not, the forces available are insufficient to lift the platform under its gravity induced weight in the laboratory.

The measurements of the platform elevation present behaviors close to those predicted by the model. The comparison leads to the conclusion that the developed tool approximates the hexapod behavior and produces satisfactory results (Fig. 17). The model simulates an ideal case in which the six legs have the same behavior inducing pure uniaxial, vertical translation ($\Delta_z \neq 0$) of the platform ($\Delta\Theta_x=\Delta\Theta_y=\Delta\Theta_z=0$ and $\Delta_x=\Delta_y=0$). Furthermore, it does not take into account the dissipation in the end-stroke devices, which have not been accurately modeled.

5 Sensitivity Analysis of the Deployment

5.1 Design of Experiments Methods. The DOE method is a well known approach used to extract parameter influence from the measurement results (see Refs. [22,23]). They are based on a general multidimensional regression tool and a statistical analysis. A full factorial design of experiments investigates the responses of any possible combination of parameter levels and analyzes the effects of the main parameters and their interactions.

In this study, the method of full factorial design is applied to simulation results. The Al Majid model parameters of each linear actuator are modified slightly to take into account uncertainties in the actuators during the deployment. Determining the parameters and their levels is the key task for a successful factorial design. Systems such as parallel structures involve multiple stages of complexity that make the system difficult to predict. The stored

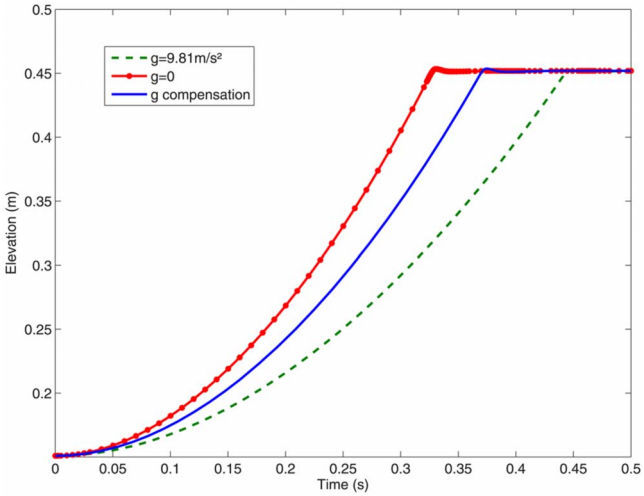

Fig. 16 Platform elevation: prediction of the gravity influence on the deployment

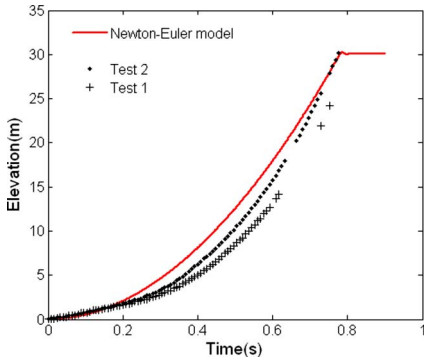

Fig. 17 Platform elevation: comparison models/measurements

Table 1 Definition of DOE parameters

Leg number	Coding letter	
	Stored effort	Asymptote slope
1	A	B
2	C	D
3	E	F
4	G	H
5	J	K
6	L	M

energy and the rate of change in uncoiling force with actuator extension, i.e., a_l and b_l, are the parameters that are perturbed (see Eq. (3)), leading to 12 parameters for the whole hexapod.

A two-level design is used, which assigns each parameter independently to either a low or a high value, leading to a generalized linear approximation. This choice can be easily understood because the number of simulations skyrockets when 12 parameters are considered, leading to 2^{12} i.e., 4096 experiments. The levels are specified by experimental uncertainties: in Fig. 7(*b*), the difference between coiling and uncoiling loads is rather small, around 0.1 N. Consequently, the selected parameters of each actuator are subjected to $\pm 10\%$ to define their low and high levels in order to describe realistic dispersions. All the cases defined by the full factorial design were introduced as different inputs of the deployment model described previously. The trajectory of the center of inertia of the upper platform was recorded during deployment at a sampling rate of 1000 Hz for a total duration of 1 s. For each simulation, the maximum values of lateral and angular deviations were recorded to analyze stability through the design of experiments.

5.2 Platform Response. The angular displacement θ_z around the vertical axis shows high fluctuation during deployment. The dynamic stability of the deployment is mostly governed by this twist motion. Typically, critical simulations lead to a torsional oscillation of amplitude θ_z greater than 30 deg, referred to as the threshold of stability. Obviously, this motion is unrealistic in this case because the prototype hexapod would collapse due to the buckling of the tape-springs. When coordinate θ_z is small enough, the other coordinates remain within a workspace where the upper platform deployment reaches its proper final position.

Examining the variation of $\Theta_z = \max(\Delta\theta_z)$ permits listing the interactions of their parameters as a function of their percentage of total variability. Results show that a slight disturbance of the stored effort on only one actuator (the other stored efforts remaining equal) could lead to deployment failure.

Broadly speaking, a regression fitted model is available and permits substantial reduction in computation time by obtaining a quasianalytical formula in order to optimize design. In this investigation, the aim was to highlight the relationship between the Θ_z response and the influential parameters that could be useful in the development of a controlled hexapod. Based on the previous results, a formula was established with the first and third order interactions,

$$\begin{aligned}\Theta_z = \varepsilon &+ 86.6(A - C + E - G + J - L) + 5.86(ACE - ACL - AEJ \\ &+ AJL - CEG + CGL + EGJ - GJL) + 5.84(-ACG + ACJ \\ &+ AEG - CJL - EGL + EJL) + 5.79(AEL + AGJ - AGL \\ &+ CEJ - CEL - CGJ) \end{aligned} \quad (6)$$

Parameters were entered in coded form (see Table 1), taking the values in a normalized range $[-1 \rightarrow 1]$ corresponding to a [2.51 N; 3.07 N] range effort when real values are considered.

The values of these effects clearly show that torsional stability is very sensitive to small perturbations of the stored effort even in only one actuator. In order to ensure a reliable deployment by confining the twist motion in an interval of a few degrees, the stored efforts should have an uncertainty less than 10^{-3} N. Moreover, one can easily imagine that such a level of accuracy in force control must be accompanied with precision positioning of the legs and actuators on the platforms.

6 Conclusion

In the framework of a future space application, this paper presents a deployable hexapod equipped with tape-spring actuators in order to carry out an analysis of the deployment behavior. The platform elevation of the prototype is performed with a gravity compensation setup and measured with a high speed camera. The manipulation of the prototype is delicate. Consequently, the experimental deployment workspace is limited to prevent excessive planar excursions that could lead to collapse. Results show that initial conditions of the platform position are decisive.

The deployment modeling of the hexapod is performed by using longitudinal phenomenological models in parallel. The originality of this investigation is that the release of stored energy and dry friction in the tape-spring actuators is described by force-elongation loops. It is achieved by using an experimental identification of a tape-spring actuator hysteresis and modeled with the Al Majid model. The hexapod raises to its final position, thanks to the combination of the parallel restoring force models and end-stops. Consequently, the model provides the dynamic behavior of the structure during deployment.

The disparity in the actuator restoring forces causes deviations compared with the ideal platform trajectory. The DOE method highlights that the twist motion around the vertical axis is detected as the main indicator of deployment failure. This means that focusing on the angular coordinate Θ_z is sufficient to ensure deployment stability. The regression model obtained predicts the twist behavior of the hexapod with disturbed legs. It will be useful for a design optimization with its inverse form and for choosing an adequate strategy of control.

Such an experiment flown in an aircraft to produce a 0 G environment might establish our techniques to be sufficiently reliable so as to be accepted as a standard verification procedure for similar mechanism designs for application in space.

References

[1] Berger, K. T., Horta, L. G., and Taleghani, B. K., 2004, "Static Testing of an Inflatable/Rigidizable Hexapod Structure," 45th AIAA/ASME/ASCE/AHS/ASC Structures, Structural Dynamics and Materials Conference, AIAA, Palm Springs, CA.

[2] Jenkins, C. H., and Kalanovic, V. D., 2000, "Issues in Control of Space Membrane Inflatable Structures," IEEE Aerospace Conference, Big Sky, MT, pp. 411–414.

[3] Tibert, G., 2002, "Deployable Tensegrity Structures for Space Applications," Ph.D. thesis, Royal Institute of Technology.

[4] Merlet, J.-P., 1997, *Les Robots Parallèles*, Hermès Science, Paris.

[5] Merlet, J.-P., 2006, "Jacobian, Manipulability, Condition Number, and Accuracy of Parallel Robots," ASME J. Mech. Des., **128**, pp. 199–206.

[6] Jiang, Q., and Gosselin, C. M., 2008, "The Maximal Singularity-Free Workspace of the Gough–Stewart Platform for a Given Orientation," ASME J. Mech. Des., **130**, p. 112304.

[7] Blanchard, L., Falzon, F., Dupuis, J., and Merlet, J. P., 2005, "Deployable Hexapod Using Tape-Springs," Disruption in Space, ESA/CNES Symposium, Marseille, France.

[8] Merlet, J.-P., 1986, "Contribution à la formalisation de la commande par retour d'effort en robotique: Application à la commande de robots parallèles," Ph.D. thesis, Université Paris 6.

[9] Mansfield, E. H., 1973, "Large-Deflexion Torsion and Flexure of Initially Curved Strips," Proc. R. Soc. London, Ser. A, **334**, pp. 279–298.

[10] Seffen, K. A., 1997, "Analysis of Structures Deployed by Tape-Springs," Ph.D. thesis, Cambridge University.

[11] Seffen, K. A., and Pellegrino, S., 1997, "Deployment of a Rigid Panel by Tape-Springs," Department of Engineering, University of Cambridge, Technical Report No. CUED/D-STRUCT/TR 168.

[12] Hesselbach, J., Helm, M. B., Kerle, H., Soetebier, S., and Krefft, M., 2001, "A Parallel Robot With Spread-Band Elements," 32nd International Symposium on Robotics, Seoul, pp. 1731–1736.

[13] Aridon, G., Blanchard, L., Rémond, D., and Dufour, R., 2006, "Modal Identification for Modeling a Deployed Tape-Spring Hexapod," 47th AIAA/ASME Structures, Structural Dynamics, and Materials Conference, Newport.

[14] Mguil-Touchal, S., Morestin, F., and Brunet, M., 1997, "Various Experimental Applications of Digital Image Correlation Method," CMEM 97 (Computational Methods and Experimental Measurements VIII), Rhodes, May 1997, pp. 45–58.
[15] Dahl, P. R., 1976, "Solid Friction Damping of Mechanical Vibration," AIAA J., **14**(12), pp. 1675–1682.
[16] Al Majid, A., and Dufour, R., 2002, "Formulation of a Hysteretic Restoring Force Model: Application to Vibration Isolation," Nonlinear Dyn., **27**, pp. 69–85.
[17] Al Majid, A., and Dufour, R., 2004, "Harmonic Response of a Structure Mounted on an Isolator Modelled With a Hysteretic Operator: Experiments and Prediction," J. Sound Vib., **277**, pp. 391–403.
[18] Michon, G., Manin, L., and Dufour, R., 2005, "Hysteretic Behavior of a Belt Tensioner: Modeling and Experimental Investigation," J. Vib. Control, **11**(9), pp. 1147–1158.
[19] Rémond, D., Neyrand, J., Aridon, G., and Dufour, R., 2008, "On the Improved Use of Chebyshev Expansion for Mechanical System Identification," Mech. Syst. Signal Process., **22**(2), pp. 390–407.
[20] Nashif, A. D., Jones, D. I. G., and Henderson, J. P., 1985, *Vibration Damping*, Wiley, New York.
[21] Aridon, G., Al Majid, A., Rémond, D., Blanchard, L., and Dufour, R., 2007, "A Direct Dynamic Model for a Space Hexapod Deployment," ASME 2007 IDETC/CIE, Las Vegas, NV, Paper No. 2007-35299.
[22] Sado, G., and Sado, M. C., 1991, *Les Plans d'Expériences: De l'Expérimentation à l'Assurance Qualité*, AFNOR, Paris.
[23] Montgomery, D. C., 2005, *Design and Analysis of Experiments*, 6th ed., Wiley, New York.